Factors that Determine Zeolite Stability in Hot Liquid Water

Lu Zhang,[†,§] Kuizhi Chen,[‡,§] Banghao Chen,[∥] Jeffery L. White,[‡,§] and Daniel E. Resasco*[,†,§]

[†]School of Chemical, Biological and Materials Engineering, University of Oklahoma, 100 East Boyd Street, Norman, Oklahoma 73019, United States

[‡]Department of Chemistry, Oklahoma State University, Stillwater, Oklahoma 74078, United States

[§]Center for Interfacial Reaction Engineering (CIRE), University of Oklahoma, 100 East Boyd Street, Norman, Oklahoma 73019, United States

[∥]Department of Chemistry & Biochemistry, Florida State University, 95 Chieftan Way, Tallahassee, Florida 32306-4390, United States

ABSTRACT: The susceptibility of zeolites to hot liquid water may hamper their full utilization in aqueous phase processes, such as those involved in biomass conversion and upgrading reactions. Interactions of zeolites with water strongly depend on the presence of hydrophilic moieties including Brønsted acid sites (BAS), extraframework cations, and silanol defects, which facilitate wetting of the surface. However, it is not clear which of these moieties are responsible for the susceptibility of zeolites to liquid water. Previous studies have offered contradictory explanations because the role of each of these characteristics has not been investigated independently. In this work, a systematic comparison has been attempted by relating crystallinity losses to the variation of each of the five zeolite characteristics that may influence their stability in liquid water, including number of BAS, Si−O−Si bonds, framework type, silanol defects, and extraframework Al. In this study, we have systematically monitored the crystallinity changes of a series of HY, H-ZSM-5, and H-β zeolite samples with varying Si/Al ratio, density of BAS, zeolite structure, and density of silanol defects upon exposure to liquid water at 200 °C. The results of this comparison unambiguously indicate that the density of silanol defects plays the most crucial role in determining susceptibility of zeolites to hot liquid water. By functionalizing the silanol defects with organosilanes, the hydrophobicity of defective zeolite is increased and the tolerance to hot liquid water is significantly enhanced.
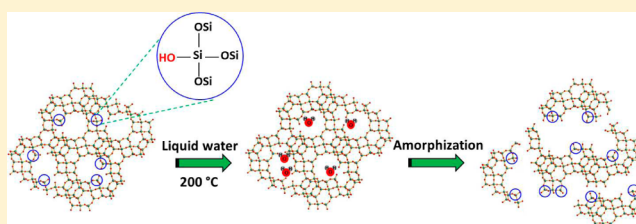
INTRODUCTION

Zeolites are remarkable microporous materials with tunable structure, acid density, and shape selectivity, which have shown unmatched performance in many vapor phase petrochemical and oil refining processes, including cracking, hydrocracking, isomerization, aromatization, etc.[1] In the vapor phase, zeolites are reasonably stable under rather severe conditions (350−500 °C).[2,3] However, it has been recently pointed out that they can be highly susceptible to hot liquid water.[4−6] This behavior is especially problematic in the case of biomass conversion and upgrading, for which acidic zeolites could become attractive catalysts due to their availability, relatively low cost, and facile property adjustability.[7] They have been found to be particularly efficient in reactions of importance in bio-oil upgrading, including dehydration, deoxygenation, alkylation, transalkylation, aldol condensation, etc.[8−13] Therefore, it is important to investigate in detail the fundamental mechanism of the liquid water attack and to determine what specific zeolite characteristics are responsible for the observed susceptibility.

Since water vapor has been widely used to modify the structure and acid density of zeolites, the interaction of water and zeolites has been investigated extensively in the past, mostly involving water in the vapor phase.[14−18] However, the thermal susceptibility of zeolites in liquid water is curiously different from that in steam. That is, while zeolites can sustain long treatments under steam at temperatures well above 500 °C, they may collapse and lose their crystallinity after only a few hours in liquid water at 200 °C. When a zeolite is exposed to water in the vapor phase at high temperature, dealumination occurs with relatively small damage to the microstructure. Under conditions of enough atom mobility, some of the Al cations move from metastable tetrahedral positions, stabilized by the framework, to more stable octahedral (extraframework) positions. During this process, only a small fraction of the microporous volume is lost, with formation of mesoscale channels. By contrast, in liquid phase, a dramatic structural collapse occurs at much lower temperatures. It is important to note that while dealumination enhances the thermal and chemical stability of zeolites in the vapor phase,[19] it seems to make the material more susceptible to attack by liquid water. In fact, recent studies[4,20] have reported dramatic crystallinity losses of dealuminated ultrastable Y (USY) zeolites in hot liquid water, which is unforeseen since these dealuminated zeolites have enhanced thermal stability in vapor phase.[21]

It is logical to expect that the interactions of zeolites with liquid water depend on the hydrophilic or hydrophobic character of the zeolite surface, which determines its wettability. This topic has received great attention during the past few years by both theorists and experimentalists.[22] For example, in a molecular simulation study of high relevance to the interaction of water in hydrophobic zeolites, Sharma and Debenedetti[23] found that the drying rate of hydrophobic cavities, simulated by two hydrophobic surfaces separated by a nanoscopic gap, increases by several orders of magnitude when the gap size is smaller than 1 nm. Therefore, while water molecules can still diffuse inside hydrophobic cavities,[24] the penetration of liquid water to hydrophobic enclosures requires exceedingly high pressures. This has been experimentally verified by Guillemot et al.,[25] who showed that when porous silica materials were fully hydrophobized, intrusion of liquid water could only occur above 500 bar. By contrast, when hydrophobic enclosures contain hydrophilic patches that can be wetted by water, they act as nucleation sites for water condensation. In fact, Giovambattista et al.[26] investigated the dynamics of water molecules within parallel plates of hydrophobic silica patterned with hydrophilic silanol (Si−OH) patches. They found that when there is an internal silanol island, water condenses around these sites and remains connected to bulk water through a chain of molecules spanning through the hydrophobic region. In another experimental study, Humplik et al.[27] found that the presence of internal silanol defects in MFI zeolites increases the amount of water adsorbed within the zeolite by up to 7 times, but lowers the diffusivity of water molecules by a factor of 2 compared to water in a nearly defect-free hydrophobic MFI zeolite. These results further support the concept that while water vapor penetrates easily in hydrophobic confinements, liquid water does not wet the surface and consequently makes intrusion much less favorable. Similarly, Ortiz-Young et al.[28] have found that the viscosity of water near solid surfaces (silica or graphene) is highly affected by the hydrophilicity of the surface. Shear viscous forces measured by an AFM tip in water are greatly increased when approaching solid surfaces at the nanoscale, and this enhancement dramatically depends on the wettability of the surface, determined by the presence of defects (silanol groups or oxidized sites). In the case of zeolites,[29] the hydrophilicity is controlled by the Si/Al ratio and the density of silanol groups. It has been recently pointed out[30] that polarity and solvating properties of zeolites can be tuned by changes in their synthesis, ranging from purely hydrophobic defect-free materials to others containing controlled amounts of hydrophilic defect sites and/or heteroatoms. In recent work, our group found that functionalizing a dealuminated HY zeolite with organosilanes renders the zeolite hydrophobic and greatly improves its stability in hot liquid water.[5] Therefore, it can be concluded that the interactions of zeolites with liquid water as well as their susceptibility to water attack should be related to hydrophilic moieties, which may include polar Brønsted acid sites (BAS), extraframework cations, and silanol defects. However, previous investigations on the susceptibility of zeolites to liquid water offer contradictory explanations. Among the possible characteristics of the zeolites that have been proposed to play a crucial role in the susceptibility to structural collapse, the following have been identified in different studies: (a) Brønsted acid sites (BAS) or Si/Al ratio, (b) Si−O−Si bonds, (c) zeolite framework type, (d) silanol defects, and (e) extraframework Al ions.

The purpose of the current contribution is to make a detailed comparison of the zeolite stability of a series of samples in which each of these characteristics is systematically varied.

■ EXPERIMENTAL SECTION

Materials and Methods. Most of the zeolites used in this study were provided by Zeolyst International. Two silicalite-1 samples, using either OH⁻ or F⁻ as mineralizing agent, were synthesized in our lab by the hydrothermal synthesis method adapted from standard procedures reported in the literature.[31,32] The zeolite specifications, product codes, and names of the samples used in this work are summarized in Table 1. The two presteamed HY 2.6 and HY 30 (CBV 600 and CBV

Table 1. Zeolite Specifications

product code	zeolite type	nominal Si/Al ratio	cation form	sample name
CBV 100	Y (FAU)	2.6	Na	NaY
CBV 300	Y (FAU)	2.6	NH₄	NH₄-Y
CBV 300	Y (FAU)	2.6	H	unsteamed HY 2.6
CBV 600	Y (FAU)	2.6	H	steamed HY 2.6
CBV 760	Y (FAU)	30	H	steamed and acid-leached HY 30
CBV 2314	ZSM-5 (MFI)	11.5	NH₄	ZSM-5
CP 814E	β (BEA)	12.5	NH₄	β
N/A	silicalite-1 (MFI)	∞	N/A	silicalite-1

760) zeolites were used as received. The three NH₄ form zeolites (CBV 300, ZSM-5, and β) were calcined at 550 °C to obtain the H form before use. The silicate-1 MFI zeolites, prepared by the two alternative routes, were calcined at 500 °C to remove the organic template (tetrapropylammonium hydroxide or tetrapropylammonium bromide).

The NaY zeolite (CBV 100) was dealuminated with SiCl₄, following the procedure proposed by Beyer et al. and DeCanio et al.[33,34] The zeolite sample was dehydrated at 300 °C for 2 h before it was heated in the flow of SiCl₄ and N₂ mixture for 3 h at 480 °C. Right after dealumination, the reaction product was treated at the same temperature for 3 h under N₂ flow to remove AlCl₃.[35] After cooling to room temperature, the sample was thoroughly washed with an excess of water. The H form of the dealuminated sample was obtained by ion exchange in a 1 M ammonium acetate solution at room temperature followed by calcination at 550 °C.

A hydrophobized zeolite was prepared by the silylation method previously described.[36] Briefly, 1 g of the parent zeolite (CBV 600) was dispersed in 20 mL of toluene by sonication with a Horn sonicator (Fisher Scientific, 600 W, 20 kHz) at 25% amplitude. Then, the zeolite suspension was added to a 50 mL solution of ethyltrichlorosilane (ETS) in toluene to get a ratio of 10 mmol ETS/g zeolite. The final suspension was stirred for 24 h at 500 rpm at room temperature. The zeolite sample was collected by filtration. After washing thoroughly with ethanol, the functionalized zeolite was dried at 100 °C.

The tests to measure the susceptibility of zeolites to hot liquid water were performed following the same procedure as that employed in our previous study.[5] That is, in each run, 0.5 g of each zeolite sample was placed in a Teflon container placed inside a 50 mL autoclave. Different amounts of water were introduced at the bottom of the same autoclave, but not directly in contact with the zeolite. Afterward, the autoclave was heated at 200 °C to generate steam at the autogenic pressure. After a specified reaction time, the autoclave was quenched with running water. The zeolite samples were collected in vials and then dried at 100 °C prior to analysis. Considering the vapor pressure (18.6 atm) and gas compressibility factor (0.96) for water at 200 °C, we determined the amount of water ($n_0 = 0.0224$ mol) required to reach the saturation of the vapor in the given autoclave volume. The n/n_0 ratio is used to represent the sum of the amount of liquid water placed in the autoclave and the amount of water already present inside

the zeolite (about 2.78 mmol for 0.5 g zeolite) relative to the number of moles at saturation (n_0). At $n/n_0 < 1$, only water vapor is present. However, capillary condensation may occur at n/n_0 values less than 1 in the small pores of the sample.

Characterization of Various Zeolites. Powder diffraction (XRD) patterns were recorded in reflection geometry on a D8 Series II X-ray diffractometer (BRUKER AXS) that uses Cu Kα radiation generated at 40 kV and 35 mA. To compare the relative crystallinity of the water-attacked samples, the standard method described in the ASTM D3906-03 was followed.[37] All the samples were stored in a hydrator, whose humidity was maintained by a saturated solution of $CaCl_2 \cdot 6H_2O$. The degree of crystallinity was estimated by comparing the area of the reflection peaks in the 2θ range 15−35° to that of the same peaks in the powder pattern of the unattacked sample.

The elemental composition of different zeolites was determined by ICP at Galbraith Laboratories. N_2 physisorption was performed on all samples on a Micromeritics ASAP 2010 unit. Prior to analysis, the samples were degassed in situ at 230 °C for 24 h. The micropore volume was derived from the t-plot method (relative pressure range: 0.2−0.6), and the total pore volume was determined at $p/p_0 = 0.99$. The mesopore size distribution was obtained by applying the BJH method to the adsorption branch of the isotherm. Raman spectra were acquired on a Jovin Yvon-Horiba Lab spectrometer, equipped with a CCD detector and a He−Ne laser (632 nm) as the excitation source. DRIFT spectra were recorded at a resolution of 4 cm^{-1}, accumulating 64 scans, on a PerkinElmer Spectrum 100 FTIR, equipped with a high temperature DRIFT cell (HVC, Harrick) with CaF_2 windows. The zeolite sample (100 mg) was loaded in the cell, heated in situ up to 300 °C under 50 mL/min He, kept at this temperature for 1 h, and cooled down to 100 °C. Before the DRIFT measurements, a background spectrum was recorded at the same resolution and number of scans.

Temperature-programmed desorption (TPD) of adsorbed iso-propylamine (IPA) was used to measure the density of Brønsted acid sites. In each measurement, 50 mg of the zeolite sample was used and pretreated for 0.5 h in He flow (20 mL/min) at 600 °C to remove any adsorbed water. Then, the sample was cooled to 100 °C under flowing He and exposed to 10 consecutive 2 μL pulses of IPA. After the samplew as flushed under He for 12 h at 100 °C to remove weakly adsorbed IPA, a 10 °C/min linear heating ramp was applied up to 600 °C. The desorbed products were analyzed and quantified on a Microvision Plus MS, scanning over a 1−60 m/z range at a speed of 26 cycles/min. The Brønsted acid density was measured from the propylene evolution ($m/z = 41$), assuming a stoichiometry BAS/propylene of 1/1 and calibrating the measured intensity with 100 μL propylene pulses.

For transmission electron microscopy (TEM), the zeolite samples were dispersed in ethanol and sonicated with a horn sonicator (Cole-Parmer), operating at 25% amplitude for 10 min before deposition onto holey carbon coated copper grids. The images were obtained on a JEOL 2000 field emission system operated at 200 kV.

^{27}Al and ^{29}Si NMR experiments were performed on a Bruker AVIII HD NMR spectrometer operating at a magnetic field strength of 11.74 T, equipped with a 4 mm Bruker MAS probe. For ^{27}Al MAS experiments, a single pulse acquisition was applied with a spinning rate of 14 kHz and a short RF pulse (less than 15°) with a recycle delay of 0.5−1 s. Spectra were collected after 10 240 scans and referenced to 1 M AlCl$_3$ aqueous solution, set at 0 ppm. For ^{29}Si MAS experiments, a single pulse acquisition (30 o RF pulse) was applied with spinning rate of 12 kHz and a recycle delay of 25 s. Spectra were obtained after 4096 scans and referenced to the TMS signal, set at −10.2 ppm.

RESULTS AND DISCUSSION

To determine exactly which zeolite characteristics determine the susceptibility to structural attack by hot liquid water, we quantified the zeolite crystallinity changes of a series of HY, H-ZSM-5 and HBEA samples with varying Si/Al ratio, density of Brønsted acid sites (BAS), zeolite structure, and density of silanol defects upon exposure to hot liquid water under

precisely controlled conditions. The resulting structural changes were characterized by powder XRD, TEM, N_2 physisorption, Raman, and MAS NMR.

Influence of the Density of BAS and Si/Al Ratio on Zeolite Susceptibility to Liquid Water. The stability of HY zeolite crystallinity with varying Si/Al ratio was tested as a function of water partial pressures and exposure to liquid water at 200 °C. The three HY samples compared in this series were a steamed HY (Si/Al = 30), a steamed HY (Si/Al = 2.6), and an unsteamed HY (Si/Al = 2.6). The HY 30 is a commercial sample (CBV 760) that has been presteamed at high temperatures and acid-leached by the manufacturer.[38] The steamed HY 2.6 is another commercial sample (CBV 600) that has been presteamed by the manufacturer.[38] In both cases, the parent sample is a NH$_4$-Y (CBV 300). For the third sample, the unsteamed HY 2.6, we used the same parent sample CBV 300 in the NH$_4$ form, without steaming, but calcined it in our lab with a 10 °C/min ramp up to 550 °C.

The relative crystallinity of the water-attacked samples is obtained by comparing the total area of the diffraction peaks in the 2θ range 15−35° to that of the same peaks in the powder pattern of the corresponding unattacked sample. The crystallinity changes of the three HY samples upon water attack are shown in Figure 1 as a function of the water
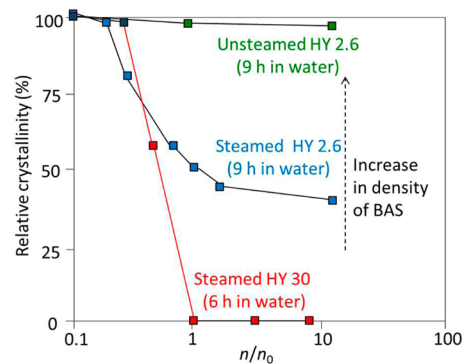
Figure 1. Percent crystallinity retained by HY zeolites with varying density of BAS after exposure to different amounts of water at 200 °C for 6 or 9 h. The n/n_0 ratio indicates the amount of water relative to that needed to saturate the vapor at 200 °C.

exposure, quantified in terms of the n/n_0 ratio. As previously pointed out,[5,6] no attack was evident for any sample when they were only exposed to water vapor at $n/n_0 < 0.3$. However, their relative crystallinities started to decrease when n/n_0 reached around 0.5. This drop can be ascribed to the capillary condensation of water in the mesopores present in the zeolites (see Table 2). From the Kelvin equation, one can calculate the mesopore diameter needed to begin having liquid water under these conditions.[6] Using a value for the surface free energy of water at 200 °C of 0.042 N/m and a molar volume of 18 cc/mol, the corresponding diameter for capillary condensation would be around 1.5 nm. We have previously proposed that condensation might begin in very small defect pockets in the zeolite crystal, and these would be the location of the initial water attack.[6] When the amount of water exceeds $n/n_0 = 1$, even by a small amount, the extent of the attack is much greater depending on the zeolite. In fact, very clear differences are observed on the different samples for $n/n_0 > 1$. The steamed (and acid-leached) HY 30 was very susceptible to liquid water attack, and its crystallinity dropped to zero after a relatively low

Table 2. Porosity Characteristics of Zeolites and Their Selected Water-Attacked Samples

sample	V_{micro} (cm^3/g)	V_{meso} (cm^3/g)	V_{meso}/V_{micro}
steamed HY 2.6	0.279	0.136	0.502
n/n_0 = 0.9	0.223	0.142	0.637
n/n_0 = 18	0.143	0.196	1.370
steamed HY 30	0.358	0.211	0.589
n/n_0 = 0.6	0.100	0.355	3.550
n/n_0 = 1.0	0	0.364	∞
unsteamed HY 2.6	0.329	0.023	0.070
n/n_0 = 18	0.309	0.056	0.181
SiCl$_4$–HY	0.230	0.028	0.122

Figure 3. Mesopore size distribution of (A) steamed HY 2.6 and (B) steamed HY 30 before and after exposure to different amounts of water.

exposure to hot liquid water (200 °C, 6 h, n/n_0 = 1.1). In contrast, the steamed HY 2.6 was somewhat less susceptible but still exhibited a significant attack. That is, the sample kept about 40−50% of its original crystallinity after about 9 h at n/n_0 ≥ 1.1. A totally different behavior was observed for the unsteamed HY 2.6, which exhibited remarkable stability in the entire n/n_0 ≥ 1.1 range. This difference will be further discussed later.

The morphological changes of the two presteamed samples after the attack are clearly evident in the TEM images of Figure 2. While both zeolites were steamed, the TEM images of the
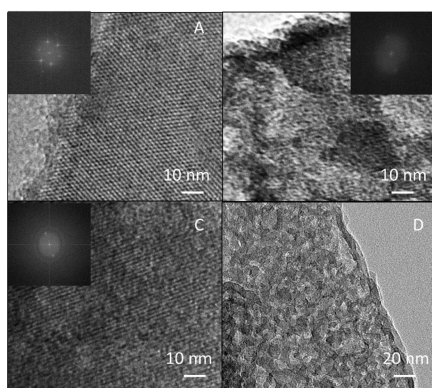
Figure 2. TEM images of steamed HY 2.6 (A) before and (B) after water attack at n/n_0 = 18. TEM images of steamed HY 30 (C) before and (D) after water attack at n/n_0 = 1.1.

steamed HY 2.6 sample show a more clear crystal structure than the HY 30 (Figure 2A,C). More interestingly, after the liquid water attack at n/n_0 = 18 (see Figure 2B), significant fragments containing a fine lattice structure were still found on the steamed HY 2.6 sample. By contrast, the drastic loss in crystallinity of the steamed (and acid-leached) HY 30 sample resulted in the generation of significant mesoporous volume, as determined by N$_2$ adsorption/desorption. Indeed, as shown in Table 2, the measured V_{meso} increased from 0.211 cm^3/g for the original HY 30 to 0.364 cm^3/g after the water attack that resulted in total loss of microporosity. The resulting changes in morphology are clearly illustrated in the TEM image of Figure 2 D. The change in V_{meso}/V_{micro} ratio is significantly smaller for the steamed HY 2.6, which as mentioned above suffered a less radical structural collapse than the HY 30 sample.

As shown in Figure 3, both steamed samples (HY 2.6 and 30) contain mesoporosity with a wide range of diameters. After the water attack, new mesopores around 10−20 and 10 nm were formed in the steamed HY 2.6 and HY 30, respectively. The greater extent of mesoporosity enhancement for HY 30
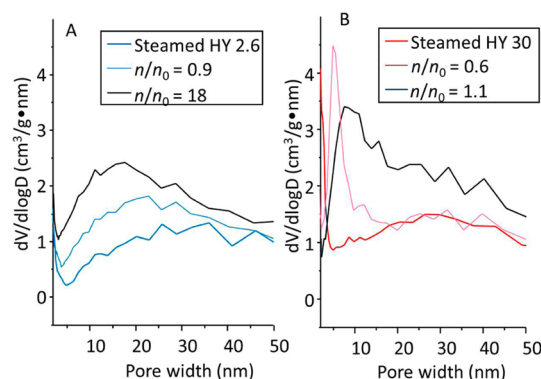
zeolite than for HY 2.6 is in good agreement with the TEM observations.

To further investigate the water attack process, Raman spectra were obtained on the steamed HY 2.6 after exposure to hot liquid water. Longer exposure times under the same n/n_0 resulted in greater losses in crystallinity, but even after 24 h at n/n_0 = 18, the steamed HY 2.6 retained about 25% of the initial crystallinity (data not shown). The Raman spectrum of the original zeolite (Figure 4) shows two strong bands at 490 and
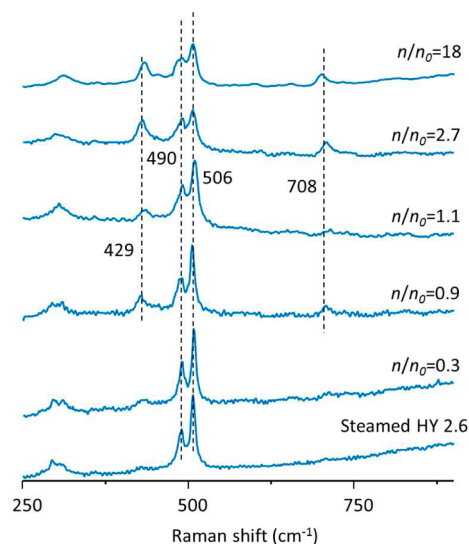

Figure 4. Raman spectra of the parent steamed HY 2.6 and the corresponding water-attacked samples at various water exposures for 24 h at 200 °C.

506 cm^{-1}, which result from the T−O−T bending modes of four-membered ring units (4Rs) in the zeolite.[39] In addition, several overlapping weaker bands are observed centered around 300 cm^{-1}; they are usually ascribed to T−O−T bending modes of 6Rs.[39] After 24 h treatments at 200 °C, the intensity of the strong bands decreased with increasing water exposure from n/n_0 = 0.3 to 1.1. This decrease in intensity parallels the crystallinity drop observed in the XRD of the attacked samples. The changes in Raman spectra upon water attack are reminiscent of some of the phenomena observed during zeolite synthesis. Indeed, on the basis of ex situ and in situ Raman studies during the formation of faujasite crystals, Li and co-workers[40,41] reported that, in the early stages of the nucleation,

an amorphous aluminosilicate (AS) phase was formed, and it was mainly composed of 4Rs. During crystallization, these 4Rs were connected with 6Rs to form sodalite cages, which reorganized with double 6Rs to form the framework of zeolite faujasite. The intensity of the 4R bands followed an S-shaped growth curve. Here, the intensity decrease of this band suggests that the water attack process can be seen as essentially a zeolite synthesis in reverse. That is, during the water attack the crystalline structure dissolves and transforms into a disordered AS phase, terminated by T−OH species. This is, in fact, supported by the appearance of new bands at 429 and 708 cm^{-1}, which can be ascribed to T−OH bending modes in the AS phase.[39]

The ^{29}Si MAS NMR spectra for steamed HY 30 and HY 2.6 and unsteamed HY 2.6 before exposure to hot liquid water are compared in Figure 5. First, we must notice that, despite the
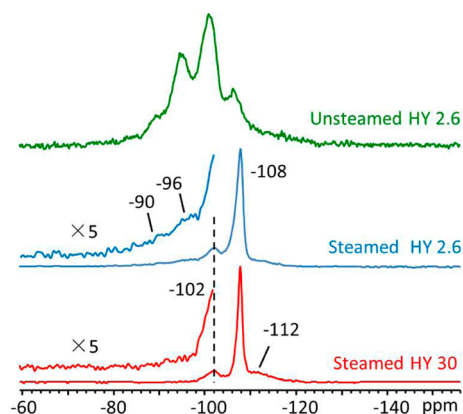
Figure 5. ^{29}Si MAS NMR spectra of original HY samples (before water attack) with varying Si/Al ratio.

dramatic difference in Si/Al ratio, the spectrum of steamed (and acid-leached) HY 30 is very similar to that of steamed HY 2.6. Both of them show a strong peak at −108 ppm and a much weaker one at −102 ppm. The former is due to Si(OSi)$_4$ species, typical of high silica zeolites. The latter could arise by the presence of one Al cation in the second coordination sphere of Si, forming Si(OAl)$_1$(OSi)$_3$. A broad halo centered at around −112 ppm in the spectrum of steamed HY 30 results from extraframework Si species. A further examination of the spectra upon magnification indicates that the steamed HY 2.6 sample also contains two weak ones at around −90 and −96 ppm, while both of them are absent in the spectrum of the steamed HY 30. They are assigned to framework Si(OAl)$_3$(OSi)$_1$ and Si(OAl)$_2$(OSi)$_2$ species, respectively.[42] From the relative intensity of these ^{29}Si peaks (−112 ppm peak is not considered), one can calculate the framework Si/Al ($F_{Si/Al}$) ratios for the two samples. As shown in Table 3, on the basis of

**Table 3. Total Si/Al Ratio As Reported by the Manufacturer**[a]

sample	$T_{Si/Al}$	$F_{Si/Al}$	density of BAS (mmol/g)
steamed HY30	30	>45	0.29
steamed HY 2.6	2.6	>20	0.45
unsteamed HY 2.6	2.6	3.0	1.05
SiCl$_4$-HY	N/A	128.8	N/A

^{a}$F_{Si/Al}$ ratio derived from ^{29}Si MAS NMR spectra. BAS obtained from IPA TPD measurements.

these ^{29}Si MAS NMR spectra, this ratio is calculated to be about 19 for the steamed HY 2.6 and about 45 for the steamed (and acid-leached) HY 30. These values can be even higher because the −102 ppm peak can also arise from Si(OSi)$_3$OH species.[43] In fact, as demonstrated later in the paper, these two samples have a significant density of silanol groups, which are evidenced by a characteristic band in the DRIFT spectra. In any case, the lower $F_{Si/Al}$ in steamed HY 2.6 compared to HY 30 suggests that it contains a higher density of BAS. Indeed, in agreement with this conclusion from the NMR data, the direct measurement of BAS by the IPA-TPD method (see Table 3) indicates that the density of BAS is 0.451 mmol/g in steamed HY 2.6, about twice as large as that in HY 30 (0.287 mmol/g). From this analysis, an important conclusion may be drawn about the link between the density of BAS and the susceptibility to water attack. That is, even though it is well-established that the density of BAS correlates well with the adsorption of water vapor it does not correlate with the zeolite susceptibility to water attack. Previous studies have shown that the adsorption capacity decreases with the severity of steaming, as BAS are lost.[44] However, we see here that a more severe dealumination does not make the zeolite less susceptible to liquid water attack.

Further confirmation for the lack of correlation between the density of BAS and the zeolite susceptibility to hot liquid water comes from the results obtained with the unsteamed HY 2.6 zeolite, which, as shown in Figure 1, is the most stable of the three. This zeolite has the lowest Si/Al ratio. Its ^{29}Si NMR spectrum exhibits four distinct signals (see Figure 5), which are typical of low-Si zeolites. It is known that, depending on the number of Al atoms in the secondary coordination sphere of the central Si atom, the ^{29}Si NMR spectrum could exhibit up to five distinct signals.[45] For each additional Al substituent, the ^{29}Si signal shifts to lower fields by about 5 ppm. That is, the presence of four ^{29}Si NMR peaks in unsteamed HY 2.6 suggests a high framework Al content. From this analysis, the $F_{Si/Al}$ ratio in this sample is calculated to be about 3.0 (Table 3), which agrees well with the high density of BAS measured by IPA (1.048 mmol/g). An interesting point that needs further discussion is the disparity between the density of BAS that one estimates from the $F_{Si/Al}$ ratio and that measured by IPA TPD. It is well-known that the IPA TPD method does not probe every Brønsted acid site in faujasites since these zeolites have BAS in both supercages and sodalite cages.[46] In a perfect faujasite crystal, only the BAS located in supercages can be probed by IPA adsorption. The six-member ring windows are not big enough to allow the IPA molecule to diffuse into the sodalite cages. As a result, the density of BAS probed by IPA is only a fraction of the theoretical value or of that estimated from framework Si/Al ratio, as measured by NMR. However, on steamed zeolites, partial destruction of the structure may open up a fraction of the sodalite cages, exposing a larger fraction of BAS compared to the case in the more perfect structure. In fact, this is observed when comparing unsteamed and steamed HY 2.6. While for the former the BAS (from IPA TPD) is 1.05 mmol/g for a framework Si/Al ratio of 3, for the latter, it only drops by about a factor of 2 (to 0.45 mmol/g) when the framework Si/Al ratio increases by a factor of 6−7. That is, the IPA TPD method in the perfect crystal may miss a large fraction of BAS inaccessible to IPA, but this fraction is lower upon steaming.

^{27}Al MAS and ^{29}Si MAS NMR spectra of steamed HY 2.6 and its water-attacked samples are shown in Figure 6. The spectrum of steamed HY 2.6 contains three resonance lines
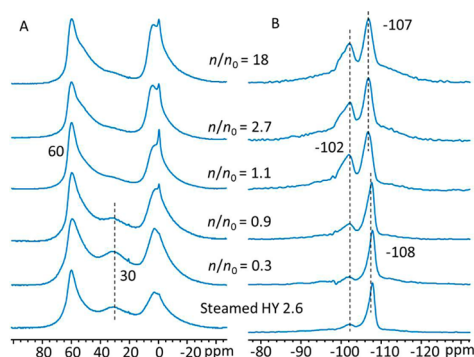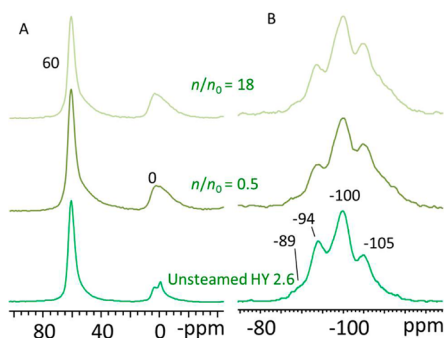
Figure 6. (A) ^{27}Al MAS and (B) ^{29}Si MAS NMR spectra of steamed HY 2.6 before and after exposure to different amounts of water for 24 h at 200 °C.

(Figure 6A). The one centered at 0 ppm is typically assigned to octahedral Al, the one at 60 ppm to tetrahedral framework Al, and the one at 30 ppm to distorted tetrahedral Al (or pentacoordinated Al).[47] The assignment of the 30 ppm peak to pentacoordinated Al may be misrepresented as in the ^{27}Al NMR, the Al species have nonspherical electron density and thus a large quadrupole coupling constant. With increasing water exposure, the octahedral/tetrahedral Al ratio exhibits an increasing trend, implying that during the water attack some tetrahedral framework Al (TFAL) cations are converted into octahedrally coordinated extraframework Al (OEFAL) cations. The sharp peak at ca. 0 ppm in the water-attacked samples has also been observed by Ennaert et al.[20] It results from OEFAL on the ion exchange positions.

As shown in the ^{29}Si MAS spectra of Figure 6 B, corresponding to the steamed HY 2.6, a significant increase in the intensity of the −102 ppm peak can be observed when n/n_0 increased from 0.3 to 18. As mentioned above, the peak at −102 ppm can be either due to Si(OAl)$_1$(OSi)$_3$ species, with an Al cation in the secondary coordination sphere, or to Si(OSi)$_3$OH species, resulting from the presence of SiOH groups. Since one cannot expect that the density of Al in the secondary coordination sphere of Si increases upon water exposure, the growth of the −102 ppm peak can be due to an increase in the number of Si−OH defects, which is consistent with the Raman spectral changes.

A very different behavior is displayed by the unsteamed HY 2.6 zeolite. In this case, as shown in Figure 7A,B, both the ^{27}Al MAS and ^{29}Si MAS spectra of the water-attacked samples are almost unchanged in comparison to those of the original

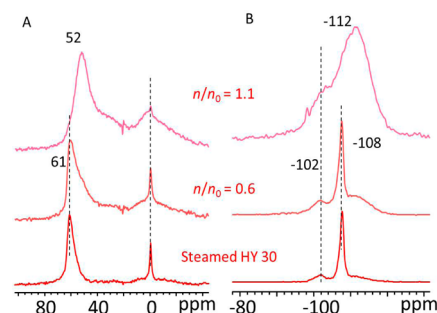**Figure 7.** (A) ^{27}Al MAS and (B) ^{29}Si MAS NMR spectra of unsteamed HY 2.6 before and after exposure to different amounts of water for 9 h at 200 °C.

sample. This stability is in perfect agreement with the crystalline stability monitored by XRD (Figure 1) and low mesopore/micropore volume ratio as measured by N$_2$ adsorption/desorption (Table 2) on this sample before and after water attack.

The ^{27}Al NMR spectrum of the steamed (and acid-leached) HY 30 before exposure to and attack by liquid water shows the characteristic peaks at 0 ppm due to the octahedral Al and at 61 ppm due to tetrahedrally coordinated extraframework Al. The narrow peak ca. 0 ppm is characteristic of acid-leached samples, such as HY 30.[48]

Interestingly, as shown in Figure 8A, despite the total loss in crystallinity of the HY 30 upon exposure to liquid water, the

Figure 8. (A) ^{27}Al MAS and (B) ^{29}Si MAS NMR spectra of the steamed HY 30 before and after exposure to different amounts of water for 6 h at 200 °C.

majority of the Al atoms remained in a tetrahedral environment. This is a remarkable result, since when removed from the framework, Al always tends to adopt the octahedral configuration. However, it must be noted that a change in chemical shift from 61 to 52 ppm is seen for the tetrahedral Al peak after the water attack.[4] Clearly, the local environment of the tetrahedral Al cations has changed due to the complete structural collapse undergone by this zeolite. Ravenelle et al.[4] have observed this transformation during the water attack of HY zeolites and ascribed the peak at 52 ppm to tetrahedral extraframework Al (TEFAL) species, which become more abundant as TFAL and OEFAL decrease.

Interestingly, the ^{29}Si NMR spectrum of this sample (Figure 8B) shows a very broad resonance line centered at −112 ppm, which results from extraframework Si(OSi)$_4$ species in the amorphous structure generated during the attack. In a recent study, Vjunov et al.[49] have interpreted the observed preservation of the tetrahedral Al cations as an indication that the hot liquid water attack does not occur at the Al sites, but rather occurs via hydrolysis of Si−O−Si bridges, which subsequently become defects and propagate the zeolite degradation. This proposal follows a similar concept previously made by Ravenelle et al.,[4] who concluded that hydrolysis of siloxane groups is the main degradation pathway since the local environment of Si was more extensively modified than that of tetrahedral Al sites.

Therefore, the first conclusion in this analysis is that the attack does not occur at the BAS, so we will focus next on the hypothesis that it might start at Si−O−Si sites.

Influence of the Si−O−Si Bonds on Zeolite Susceptibility to Liquid Water. As shown above, the most susceptible of the three HY zeolites investigated was HY 30, which is dealuminated by steaming and further acid-leached to remove some of the extraframework Al cations, resulting in a very high

Si/Al ratio and presumably a high density of Si−O−Si linkages. What is not clear is whether these linkages are particularly susceptible to water attack. It is known that dealumination by steaming and acid-leaching may cause structural damage to the zeolite. Therefore, for an independent investigation of the susceptibility of Si−O−Si linkages to water attack, with avoidance of steaming or acid-leaching, a high-silica HY was prepared by dealumination with $SiCl_4$ vapor.

In this method, framework vacancies are created by the removal of framework Al atoms that react with $SiCl_4$, but they are rapidly healed by Si from $SiCl_4$.[33,50,51] Therefore, a high Si/Al ratio zeolite is obtained without detriment in crystallinity. In fact, the resulting framework Si/Al ratio estimated from the ^{29}Si MAS NMR spectrum of this sample (see Figure 9B) is

Figure 10. TEM images of (A) $SiCl_4$-HY and (B) water-attacked sample at $n/n_0 = 5.0$ for 6 h.
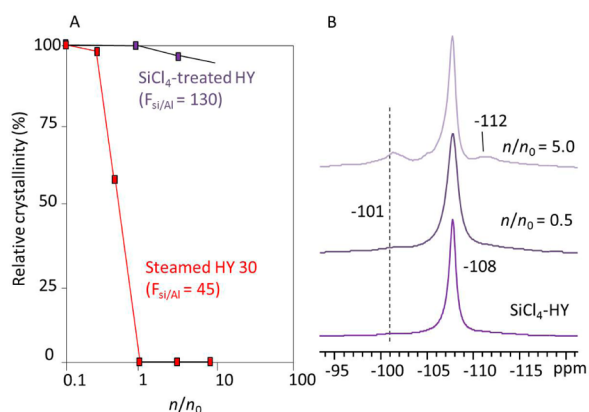
Figure 9. (A) Stability comparison between steamed HY 30 and $SiCl_4$-treated HY samples and (B) ^{29}Si MAS NMR spectra of $SiCl_4$-HY and its water-attacked samples. They were tested at various n/n_0 ratios for 6 h.

approximately 130 (Table 3). That is, this sample should contain a very high density of Si−O−Si links, which have been proposed to be the sites where water attack starts. However, this sample is not susceptible to hot liquid water, but on the contrary, the sample is very stable. A direct comparison of the stability of the $SiCl_4$-treated HY 130 with the steamed and acid-leached HY 30 upon attack with liquid water is made in Figure 9A. The difference is remarkable; while the $SiCl_4$-treated HY 130 zeolite essentially kept its original crystallinity unaffected upon exposure to water at $n/n_0 = 5.0$, the HY 30 became completely amorphous under the same conditions. In good agreement with the high stability revealed by XRD, the ^{29}Si MAS NMR spectra of $SiCl_4$-treated HY 130 before and after exposure to water showed very small differences (Figure 9B); only slight increases were observed in the intensity of the peaks due to SiOH groups (−102 ppm) and extraframework silica (−112 ppm). Moreover, the TEM image of the $SiCl_4$-treated HY 130 zeolite depicted in Figure 10A illustrates the highly crystalline structure of this sample, without the mesopores typically observed in steam-dealuminated high-silica HY zeolites.[52] This is also confirmed by the low V_{meso}/V_{micro} ratio from the N_2 adsorption/desorption measurement (0.122, Table 2). At the same time, the TEM image of the water-attacked sample ($n/n_0 = 5.0$) gives further evidence to the preservation of the crystalline structure, showing only a slight attack, most probably localized at the external surface of the zeolite (Figure 10B). These images fully agree with the ^{29}Si NMR and XRD, which prove the low susceptibility of this sample to hot liquid
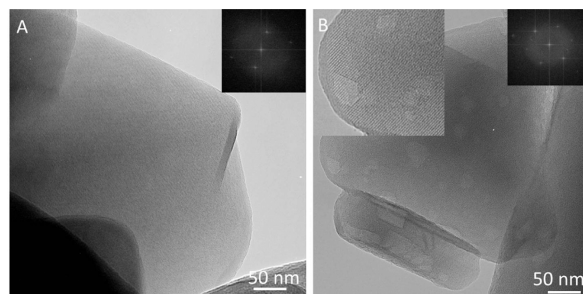
water. This experiment eliminates Si−O−Si bonds as potential site of water attack.

Influence of the Framework Type on Zeolite Susceptibility to Liquid Water. It has been widely proposed that the type of zeolite framework has a strong effect on the susceptibility of the material to liquid water.[4] It has been shown that ZSM-5 (MFI) and mordenite (MOR) zeolites are more stable than HY (FAU) or β (BEA) zeolites.[17] The higher stability of the former two types of zeolites has been linked to their denser framework.[17] Similarly, Ravenelle et al.[4] found that H-ZSM-5 is more stable than faujasite in the presence of hot liquid water, and they ascribed this enhanced stability to the differences in the zeolite framework type due to differences in the intrinsic thermodynamic stability or density of the material.[53]
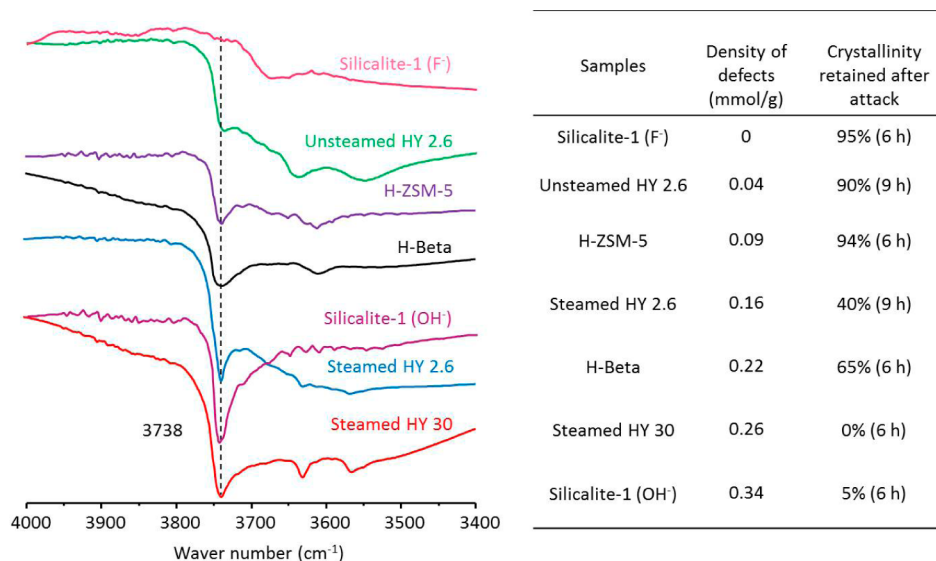
However, as illustrated in Figure 11, both FAU and MFI zeolites can be stable or unstable depending on the synthesis and postsynthesis methods rather than the zeolite framework. That is, as shown above, steamed HY 2.6 is rather unstable in liquid water, losing about 60% crystallinity upon water attack (Figure 11A).

By contrast, an unsteamed HY 2.6, with the same framework, can be very stable in liquid water. A more direct comparison can be made with two pure-silica MFI zeolites synthesized by two different methods, using hydroxide or fluoride medium. As shown in Figure 11, the silicalite-1 product made by the fluoride route presented a very high stability upon exposure to water while the one from the hydroxide route was very unstable and lost over 90% of its original crystallinity when exposed to hot liquid water. It is known that the former one has a low level of defects while the latter contains many defects. It is then clear that water susceptibility is not governed by the zeolite framework by itself, but rather by the density of defects (silanols), which greatly depends on the synthesis or postsynthesis method employed. This point is further supported by the water attack results on H-ZSM-5 and H-β. Both of them have a denser framework than faujasite. However, the former was very stable under the attack, while the latter lost near 40% of the original crystallinity when exposed to liquid water.

Influence of the Density of Defects (Silanols) on Zeolite Susceptibility to Liquid Water. After eliminating the Si/Al ratio, density of BAS, Si−O−Si linkages, and zeolite framework type as potentially determining factors of the susceptibility to hot liquid water, we now concentrate on the role of framework defects, in particular, silanols (Si−OH). The DRIFT technique is particularly suitable to quantify the density of silanol groups on a zeolite.[54] Figure 12 shows the DRIFT spectra of the various zeolites investigated in this work along with the % crystallinity retained in each zeolite after the water
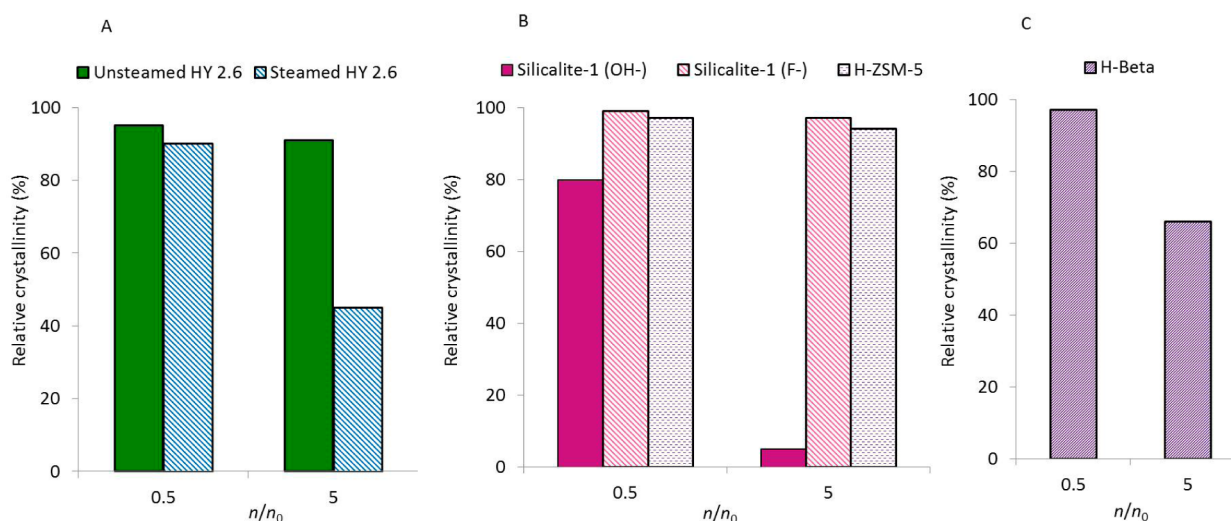
Figure 11. Percent crystallinity retained in zeolite HY (FAU framework, A), silicalite-1 and H-ZSM-5 (MFI framework, B), and H-β (BEA framework, C) upon water attack at 200 °C. Steamed and unsteamed HY 2.6 were tested for 9 h and all the other samples for 6 h.

Samples	Density of defects (mmol/g)	Crystallinity retained after attack
Silicalite-1 (F⁻)	0	95% (6 h)
Unsteamed HY 2.6	0.04	90% (9 h)
H-ZSM-5	0.09	94% (6 h)
Steamed HY 2.6	0.16	40% (9 h)
H-Beta	0.22	65% (6 h)
Steamed HY 30	0.26	0% (6 h)
Silicalite-1 (OH⁻)	0.34	5% (6 h)

Figure 12. DRIFT spectra of different zeolites before water exposure and % crystallinity retained after hot liquid water attack.

attack. It is clear that the four bottom spectra, corresponding to steamed HY 2.6, HY 30, silicalite-1 (OH⁻), and H-β all contain an intense band around 3738 cm⁻¹, which is typically ascribed to single and germinal silanol groups (SiOH).[55] The strong intensity of this band reflects the high density of defects, terminated by Si−OH silanols, in these three zeolites. The table in Figure 12 clearly shows that the susceptibility of these four samples to hot liquid water attack is very high. In fact, all of them displayed significant crystallinity losses after exposure to liquid water at 200 °C. By contrast, the three top DRIFT spectra, corresponding to H-ZSM-5, unsteamed HY 2.6, and silicalite-1 (F⁻), show much weaker bands in this region, which is consistent with the remarkable stability of these two samples. Their crystallinity remained over 90% after the water attack. To quantify the density of defects in these samples the steamed HY 30 was used as the basis for comparison. Our previous work has shown that the silanol density in the steamed HY 30 is about 0.26 mmol/g.[6] Accordingly, the SiOH defect density in all other samples was obtained from the normalized DRIFT band area for SiOH groups compared to that in steamed HY 30. The

table in Figure 12 shows a clear correlation between defect density and stability. Samples with SiOH group density of about 0.1 mmol/g or less are highly stable when exposed to hot liquid water. However, when the density is above 0.25 mmol/g, the zeolites drastically lose crystallinity in hot liquid water. Zeolites with intermediate defect density only show partial losses in crystallinity.

Therefore, the important conclusion that can be finally drawn is that the density of defects in the zeolite is the most crucial factor that determines stability in hot liquid water. Silanols not only provide a hydrophilic patch where water molecules can nucleate and wet the surface, but also are more reactive toward water, making the hydrolysis process easier. By contrast, Si−O−Si sites neither provide hydrophilicity nor high reactivity toward hydrolysis. Similarly, Al−O−Si (or BAS) sites do not seem to be reactive enough. As shown above and pointed out by Vjunov et al.[49] a large fraction of the Al cations retain their tetrahedral coordination, even after extensive water attack and total loss of crystallinity.

Participation of EFAL Species in the Stabilization of the Zeolite Structure During the Water Attack. After determining that Si−OH defects are the main characteristics of the zeolite responsible for the water susceptibility, we should discuss in this context the role of EFAL species in the stability of zeolites in liquid water. Previous studies have shown that the presence of EFAL somehow inhibits the water attack. Ennaert et al.[20] have observed that, during exposure to hot liquid water, the Al species are not dissolved, but rather remain in the solid, preferentially deposited on the outer surface and on the walls of the mesopores. These authors suggest that, after the initial attack, the EFAL species partially stabilize the zeolite, inhibiting further attack. This concept is in agreement with the preceding studies by Lutz et al.,[14] who suggested that, upon steaming under hydrothermal conditions, extraframework Al species formed a protective surface layer that blocked the terminal Si−OH groups enhancing the stability of the zeolite. Therefore, it can be concluded that the observed stabilizing effects of EFAL species can be described as a simple capping of the reactive defects. However, this capping is not entirely selective or fully efficient. By contrast, functionalization with an organosilane that selectively reacts with every exposed Si−OH species can be much more effective. This methodology is discussed below.

Effective Enhancement of Zeolite Stability in Liquid Water by Hydrophobization with Organosilanes. Since the stability of zeolites in hot liquid water is directly related to the presence of SiOH terminated defects, enhanced tolerance can be achieved by functionalizing these defects with organosilane reagents, which cap the Si−OH groups and render the zeolite hydrophobic, as recently demonstrated in our previous studies.[5,6]

Here, we compare the effect of silylation on one of the zeolites in the series (steamed HY 2.6) that has shown relatively low stability in hot liquid water. First, the DRIFT spectra included in Figure 13A demonstrate that the silylation
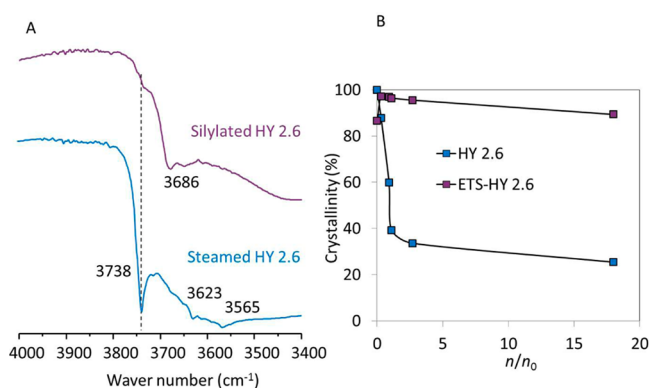
Figure 13. Comparison of DRIFT spectra and crystallinity losses in steamed HY 2.6 and its silylated form upon water attack.

method selectively titrates the silanol groups; clearly, the intensity of the 3738 cm^{-1} band is much weaker in the silylated HY 2.6 sample than in the original steamed HY 2.6, indicating an effective capping of the majority of the silanol groups by the organosilane used in this case, ethyltrichlorosilane (ETS). The two peaks at around 3623 and 3565 cm^{-1} are associated with the BAS in the supercages and those inside the sodalite cages, respectively.[56] They are not reacted with the organosilane, demonstrating the high selectivity of the method. While the ETS reagent was used in excess to achieve full functionalization

of the silanols, the presence of extraframework alumina inside the pores, as shown by NMR, may have prevented the complete reaction between silanols and ETS. Then, a new band observed at 3686 cm^{-1} in the spectrum of the silylated HY 2.6 may be due to the interaction of the unreacted silanols with residual alkyl groups from the organosilane.[5] In any case, the functionalization is effective enough to greatly enhance the tolerance of the zeolite to hot liquid water. In fact, as shown in Figure 13B, the silylated HY 2.6 after several hours in hot liquid water practically retained the same crystallinity as before the attack; by contrast, the steamed HY 2.6 lost almost 50% of the original crystallinity.

■ CONCLUSIONS

A systematic comparison of the stability of a zeolite series with varying bulk Si/Al ratios, framework type, and synthesis and postsynthesis methods, has allowed us to unequivocally demonstrate that the main characteristic of the zeolite that determines its susceptibility to hot liquid water is the density of silanol-terminated defects. The water attack experiments on unsteamed HY(2.6), a sample that has an almost defect-free structure, indicate that, with the absence of defects, zeolites could maintain high crystallinity in the presence of hot liquid water. The conclusion is further confirmed by the behavior of a high-silica HY zeolite with a framework Si/Al ratio of about 130 prepared by chemical dealumination with SiCl$_4$ which is also defect-free. This sample kept the structural integrity upon exposure to water. That is, neither high nor low Si/Al ratios cause low stability when the zeolite has no defects.

By contrast, the presteamed samples (HY 30 and HY 2.6) with a high density of silanol-terminated defects exhibited severe crystallinity losses. The same role of defects was observed in other types of zeolites, e.g., MFI. That is, the silicalite-1(OH$^-$), prepared by the hydroxide method, contained a large number of defects and was highly vulnerable to water attack. By contrast, the silicalite-1(F$^-$) prepared by the fluoride method was practically defect-free and as a result showed exceptional stability in liquid water.

The tolerance of defective zeolites to hot liquid water can be greatly enhanced by functionalization with organosilanes. This method renders the zeolite hydrophobic, which prevents the wetting of the surface. At the same time, the organosilanes act as a capping agent of Si−OH species reducing their reactivity. Both aspects are important in preventing water attack.

■ AUTHOR INFORMATION

Corresponding Author
*resasco@ou.edu
Notes
The authors declare no competing financial interest.

■ REFERENCES

(1) Degnan, T. F., Jr *Top. Catal.* **2000**, *13*, 349.
(2) Cruciani, G. *J. Phys. Chem. Solids* **2006**, *67*, 1973.

(3) Huber, G. W.; Iborra, S.; Corma, A. *Chem. Rev.* **2006**, *106*, 4044.

(4) Ravenelle, R. M.; Schüßler, F.; D'Amico, A.; Danilina, N.; van Bokhoven, J. A.; Lercher, J. A.; Jones, C. W.; Sievers, C. *J. Phys. Chem. C* **2010**, *114*, 19582.

(5) Zapata, P. A.; Huang, Y.; Gonzalez-Borja, M. A.; Resasco, D. E. *J. Catal.* **2013**, *308*, 82.

(6) Zapata, P. A.; Faria, J.; Ruiz, M. P.; Jentoft, R. E.; Resasco, D. E. *J. Am. Chem. Soc.* **2012**, *134*, 8570.

(7) Mihalcik, D. J.; Mullen, C. A.; Boateng, A. A. *J. Anal. Appl. Pyrolysis* **2011**, *92*, 224.

(8) Zhang, L.; Pham, T. N.; Faria, J.; Resasco, D. E. *Appl. Catal., A* **2014**, DOI: 10.1016/j.apcata.2014.11.018.

(9) Zhu, X.; Lobban, L. L.; Mallinson, R. G.; Resasco, D. E. *J. Catal.* **2011**, *281*, 21.

(10) Sooknoi, T.; Danuthai, T.; Lobban, L. L.; Mallinson, R. G.; Resasco, D. E. *J. Catal.* **2008**, *258*, 199.

(11) Prasomsri, T.; To, A. T.; Crossley, S.; Alvarez, W. E.; Resasco, D. E. *Appl. Catal., B* **2011**, *106*, 204.

(12) Hoang, T. Q.; Zhu, X.; Lobban, L. L.; Resasco, D. E.; Mallinson, R. G. *Catal. Commun.* **2010**, *11*, 977.

(13) Zhu, X.; Mallinson, R. G.; Resasco, D. E. *Appl. Catal., A* **2010**, *379*, 172.

(14) Lutz, W.; Gessner, W.; Bertram, R.; Pitsch, I.; Fricke, R. *Microporous Mater.* **1997**, *12*, 131.

(15) Lutz, W.; Rüscher, C.; Heidemann, D. *Microporous Mesoporous Mater.* **2002**, *55*, 193.

(16) Lutz, W.; Rüscher, C.; Gesing, T. M.; Stöcker, M.; Vasenkov, S.; Freude, D.; Gläser, R.; Berger, C. *Stud. Surf. Sci. Catal.* **2004**, *154*, 1411.

(17) Lutz, W.; Toufar, H.; Kurzhals, R.; Suckow, M. *Adsorption* **2005**, *11*, 405.

(18) Chen, K.; Damron, J.; Pearson, C.; Resasco, D.; Zhang, L.; White, J. L. *ACS Catal.* **2014**, *4*, 3039.

(19) Xu, R.; Pang, W.; Yu, J.; Huo, Q.; Chen, J. *Chemistry of Zeolites and Related Porous Materials: Synthesis and Structure*; Wiley: Singapore, 2007.

(20) Ennaert, T.; Geboers, J.; Gobechiya, E.; Courtin, C. M.; Kurttepeli, M.; Houthoofd, K.; Kirschhock, C. E.; Magusin, P. C.; Bals, S.; Jacobs, P. A.; Sels, B. F. *ACS Catal.* **2015**, *5*, 754.

(21) Scherzer, J.; Gruia, A. J. *Hydrocracking Science and Technology*; Marcel Dekker: New York, 1996.

(22) Gounder, R. *Catal. Sci. Technol.* **2014**, *4*, 2877.

(23) Sharma, S.; Debenedetti, P. G. *Proc. Natl. Acad. Sci. U. S. A.* **2012**, *109*, 4365.

(24) Striolo, A.; Chialvo, A.; Gubbins, K.; Cummings, P. *J. Chem. Phys.* **2005**, *122*, 234712.

(25) Guillemot, L.; Biben, T.; Galarneau, A.; Vigier, G.; Charlaix, É. *Proc. Natl. Acad. Sci. U. S. A.* **2012**, *109*, 19557.

(26) Giovambattista, N.; Debenedetti, P. G.; Rossky, P. J. *J. Phys. Chem. C* **2007**, *111*, 1323.

(27) Humplik, T.; Raj, R.; Maroo, S. C.; Laoui, T.; Wang, E. N. *Langmuir* **2014**, *30*, 6446.

(28) Ortiz-Young, D.; Chiu, H.-C.; Kim, S.; Voïtchovsky, K.; Riedo, E. *Nat. Commun.* **2013**, *4*, 2482.

(29) Corma, A. *J. Catal.* **2003**, *216*, 298.

(30) Gounder, R.; Davis, M. E. *AIChE J.* **2013**, *59*, 3349.

(31) Ren, N.; Yang, Z.-J.; Lv, X.-C.; Shi, J.; Zhang, Y.-H.; Tang, Y. *Microporous Mesoporous Mater.* **2010**, *131*, 103.

(32) Mallon, E. E.; Jeon, M. Y.; Navarro, M.; Bhan, A.; Tsapatsis, M. *Langmuir* **2013**, *29*, 6546.

(33) Beyer, H. K.; Belenykaja, I. M.; Hange, F.; Tielen, M.; Grobet, P. J.; Jacobs, P. A. *J. Chem. Soc., Faraday Trans. 1* **1985**, *81*, 2889.

(34) DeCanio, S. J.; Sohn, J. R.; Fritz, P. O.; Lunsford, J. H. *J. Catal.* **1986**, *101*, 132.

(35) Triantafillidis, C. S.; Vlessidis, A. G.; Evmiridis, N. P. *Ind. Eng. Chem. Res.* **2000**, *39*, 307.

(36) Singh, R.; Dutta, P. K. *Microporous Mesoporous Mater.* **1999**, *32*, 29.

(37) *ASTM Standard D3906-03, Standard Test Method for Determination of Relative X-Ray Diffraction Intensities of Faujasite-Type Zeolite-Containing Materials*, 2007.

(38) Levecque, P.; Gammon, D. W.; Jacobs, P.; De Vos, D.; Sels, B. *Green Chem.* **2010**, *12*, 828.

(39) Chen, J.; Feng, Z.; Ying, P.; Li, C. *J. Phys. Chem. B* **2004**, *108*, 12669.

(40) Xiong, G.; Yu, Y.; Feng, Z.-C.; Xin, Q.; Xiao, F.-S.; Li, C. *Microporous Mesoporous Mater.* **2001**, *42*, 317.

(41) Fan, F.; Feng, Z.; Li, G.; Sun, K.; Ying, P.; Li, C. *Chem. - Eur. J.* **2008**, *14*, 5125.

(42) Engelhardt, G.; Lohse, U.; Samoson, A.; Mägi, M.; Tarmak, M.; Lippmaa, E. *Zeolites* **1982**, *2*, 59.

(43) Dorémieux-Morin, C.; Martin, C.; Brégeault, J.-M.; Fraissard, J. *Appl. Catal.* **1991**, *77*, 149.

(44) Olson, D.; Haag, W.; Borghard, W. *Microporous Mesoporous Mater.* **2000**, *35*, 435.

(45) Lippmaa, E.; Mägi, M.; Samoson, A.; Tarmak, M.; Engelhardt, G. *J. Am. Chem. Soc.* **1981**, *103*, 4992.

(46) Farneth, W.; Gorte, R. *Chem. Rev.* **1995**, *95*, 615.

(47) Remy, M.; Stanica, D.; Poncelet, G.; Feijen, E.; Grobet, P.; Martens, J.; Jacobs, P. *J. Phys. Chem.* **1996**, *100*, 12440.

(48) Hunger, M. NMR Spectroscopy for the Characterization of Surface Acidity and Basicity. In *Handbook of Heterogeneous Catalysis*, 2nd ed.; Ertl, G., Knoezinger, H., Schueth, F., Weitkamp, J., Eds.; Wiley-VCH: Weinheim, 2008; Vol. 2, Chapter 3.2.4.4, pp 1163−1178.

(49) Vjunov, A.; Fulton, J. L.; Camaioni, D. M.; Hu, J. Z.; Burton, S. D.; Arslan, I.; Lercher, J. A. *Chem. Mater.* **2015**, *27*, 3533.

(50) Elliott, C. H., Jr.; Mcdaniel, C. V. U.S. Patent 3,639,099, 1972.

(51) Sulikowski, B.; Klinowski, J. *J. Chem. Soc., Faraday Trans.* **1990**, *86*, 199.

(52) Janssen, A.; Koster, A.; De Jong, K. *J. Phys. Chem. B* **2002**, *106*, 11905.

(53) Petrovic, I.; Navrotsky, A.; Davis, M. E.; Zones, S. I. *Chem. Mater.* **1993**, *5*, 1805.

(54) Ide, M.; El-Roz, M.; De Canck, E.; Vicente, A.; Planckaert, T.; Bogaerts, T.; Van Driessche, I.; Lynen, F.; Van Speybroeck, V.; Thybault-Starzyk, F. *Phys. Chem. Chem. Phys.* **2013**, *15*, 642.

(55) Tripp, C.; Hair, M. *Langmuir* **1995**, *11*, 1215.

(56) Parker, L.; Bibby, D.; Burns, G. *Zeolites* **1991**, *11*, 293.